HHS Public Access

Author manuscript

FASEB J. Author manuscript; available in PMC 2024 December 01.

Published in final edited form as:

FASEB J. 2023 December ; 37(12): e23275. doi:10.1096/fj.202301475R.

Loss of function of ribosomal protein L13a blocks blastocyst formation and reveals a potential nuclear role in gene expression

Ravinder Kour[1], **Jaehwan Kim**[2], **Antara Roy**[1], **Brian Richardson**[3], **Mark J. Cameron**[3], **Jason G. Knott**[2], **Barsanjit Mazumder**[1]

[1]Center for Gene Regulation in Health and Disease, Department of Biological Geological and Environmental Sciences, Cleveland State University, Cleveland, Ohio, USA

[2]Developmental Epigenetics Laboratory, Department of Animal Science, Reproductive and Developmental Sciences Program, Michigan State University, East Lansing, Michigan, USA

[3]Department of Population and Quantitative Health Sciences, Institute for Computational Biology, School of Medicine, Case Western Reserve University, Cleveland, Ohio, USA

Abstract

Ribosomal proteins play diverse roles in development and disease. Most ribosomal proteins have canonical roles in protein synthesis, while some exhibit extraribosomal functions. Previous studies in our laboratory revealed that ribosomal protein L13a (RPL13a) is involved in the translational silencing of a cohort of inflammatory proteins in myeloid cells. This prompted us to investigate the role of RPL13a in embryonic development. Here we report that RPL13a is required for early development in mice. Crosses between *Rpl13a*+/− mice resulted in no *Rpl13a*−/− offspring. Closer examination revealed that *Rpl13a*−/− embryos were arrested at the morula stage during preimplantation development. RNA sequencing analysis of *Rpl13a*−/− morulae revealed widespread alterations in gene expression, including but not limited to several genes encoding proteins involved in the inflammatory response, embryogenesis, oocyte maturation, stemness, and pluripotency. Ex vivo analysis revealed that RPL13a was localized to the cytoplasm and nucleus between the two-cell and morula stages. RNAi-mediated depletion of RPL13a phenocopied *Rpl13a*−/− embryos and knockdown embryos exhibited increased expression of *IL-7* and *IL-17* and decreased expression of the lineage specifier genes *Sox2*, *Pou5f1*, and *Cdx2*. Lastly, a protein–protein interaction assay revealed that RPL13a is associated with chromatin, suggesting an extra ribosomal function in transcription. In summary, our data demonstrate that RPL13a is essential for

Correspondence: Barsanjit Mazumder, Center for Gene Regulation in Health and Disease, Department of Biological Geological and Environmental Sciences, Cleveland State University, Cleveland, OH, USA., b.mazumder@csuohio.edu.
Ravinder Kour and Jaehwan Kim co-first author.

AUTHOR CONTRIBUTIONS

Ravinder Kour and Jaehwan Kim took a leading role in the experiments. Antara Roy contributed to some of the experiments involving gene expression analysis. Barsanjit Mazumder and Jason G. Knott conceptualized most of the studies, wrote the manuscript, and were involved in overall planning. Brian Richardson and Mark J. Cameron took a major role in bulk RNA sequence and Bioinformatics-based analysis.

DISCLOSURES

The authors declare no conflict of interest.

SUPPORTING INFORMATION

Additional supporting information can be found online in the Supporting Information section at the end of this article.

the completion of preimplantation embryo development. The mechanistic basis of the absence of RPL13a-mediated embryonic lethality will be addressed in the future through follow-up studies on ribosome biogenesis, global protein synthesis, and identification of RPL13a target genes using chromatin immunoprecipitation and RNA-immunoprecipitation-based sequencing.

Keywords

blastocyst; bulk RNA sequencing; chromatin association; embryonic development; inflammation; morula; ribosomal protein L13a

1 | INTRODUCTION

The transformation of a totipotent zygote into an implantation-competent blastocyst is a milestone of mammalian embryonic development. The window of preimplantation development involves a series of overlapping cellular and molecular events that culminate in blastocyst formation. These include depletion of maternal mRNAs, genome activation, polarization, compaction, and lineage formation.[1]

Development from the one-cell to the blastocyst stage involves global changes in gene expression and protein synthesis that prepare the embryo for implantation.[2–4] Regulation of protein synthesis by ribosomes plays a critical role in the temporal modulation of gene expression during embryonic development.[5,6] Recent studies have highlighted the role of ribosome biogenesis in embryonic brain development[7] and stem cell differentiation.[8] The regulation of embryonic development is not only achieved through the intact ribosome but also through the individual components of the protein synthesis machinery, such as ribosomal proteins.[9] A highly diverse role of many ribosomal proteins in different stages of embryonic development is emerging from the work of various laboratories. For example, the roles of RPL38[10] in skeletal pattern formation and RPLP1 in the development of the nervous system[11] are notable among these functions. Deficiencies of ribosomal proteins have been implicated in various ribosomopathies[12,13] and defects in T-cell development.[14] Insertional inactivation of L13a in drosophila causes a minute phenotype. This is a post-hatching defect that is characterized by short and slender bristles, extended developmental time, and reduced fertility.[15] However, the role of individual ribosomal proteins, such as L13a (RPL13a), during preimplantation embryo development of mammals was not reported previously.

Our previous work showed that RPL13a in mature cells is not required for the protein synthesis activity of the ribosome.[16] However, in myeloid cells, RPL13a is required for the translational silencing of a cohort of inflammatory proteins.[17] This involves the IFN-γ induced and phosphorylation-dependent release of RPL13a from the 60S ribosomal subunit followed by its assembly into a multi-protein RNA-binding complex (IFN-gamma-activated-inhibitor of translation) or “GAIT” complex on the structurally conserved RNA elements harbored in the 3′ untranslated region (UTR) of target mRNAs.[17–20] Moreover, we successfully recapitulated the consequences of the depletion of RPL13a in myeloid cells in an animal model of myeloid-specific *Rpl13a*-KO mice without any embryonic lethality. These conditional KO animals showed severe inflammation and disease outcome compared to controls using three murine models of human diseases caused by inflammation, for

example, lipopolysaccharide (LPS) induced endotoxemia,[21] high-fat diet (HFD) induced atherosclerosis,[22,23] and dextran sodium sulfate (DSS) induced colitis.[24,25] These studies motivated us to test the consequences of the systemic deletion of *Rpl13a* in whole animals.

Here, we report that systemic deletion of *Rpl13a* resulted in early embryonic lethality. In the preimplantation embryos, the *Rpl13a* null allele was able to develop up to the morula stage but then became lethal upon transition to the blastocyst stage. RNA sequencing (RNAseq) analysis of *RPL13a*−/− morulae revealed widespread alterations in gene expression and related pathways, including several genes encoding proteins involved in inflammatory response, embryogenesis, oocyte maturation, stemness, and pluripotency. Ex-vivo studies involving RNAi-mediated depletion of RPL13a in preimplantation embryos blocked blastocyst development, closely mirroring the phenotype of *Rpl13a*−/− embryos. We also found that the distribution of RPL13a protein changes during preimplantation development. At the two-cell, eight-cell, and morula stages, RPL13a is localized to both the nucleus and cytoplasm, and then during the morula-to-blastocyst transition, RPL13a becomes downregulated and localized exclusively in the cytoplasm. Lastly, studies using an in situ protein–protein interaction assay revealed that nuclear RPL13a is associated with chromatin and binds to key transcriptional regulators. Taken together, our work identifies a novel function of RPL13a during early embryonic development. This work serves as a foundation for future mechanistic studies on the precise role of RPL13a in gene expression through follow-up studies on ribosome biogenesis and global protein synthesis at the single embryo level and through the identification of RPL13a target genes by chromatin immunoprecipitation (ChIP) and RNA-immunoprecipitation (RIP)-based sequencing.

2 | MATERIALS AND METHODS

2.1 | Mice

All experiments using mice were in accordance with institutional guidelines and in compliance with the US National Research Council's Guide for the Care and Use of Laboratory Animals, the US Public Health Service's Policy on Humane Care and Use of Laboratory Animals and Guide for the Care and Use of Laboratory Animals. All animal protocols used in this study were approved by the Institutional Animal Care and Use Committee (IACUC).

2.2 | Generation of mice harboring the heterozygous null allele of L13a

See supplementary methods.

2.3 | Embryo harvesting, genotyping, and RNA isolation

Embryos at the two-cell, morula, and blastocyst stages were collected from the superovulated mice following the previously published methods.[26] Briefly, female C57bl/6 wild-type or heterozygous KO of *Rpl13a* (*Rpl13a−/+*) were injected with 5 IU of PMSG (Pregnant Mare's Serum Gonadotropin Cat# RP1782721000, Bio Vendor). After 48 h of PMSG injection, mice were injected with 5 IU of HCG (Human Chorionic Gonadotropin Cat# C1063 Sigma Aldrich) and paired with the male mice of the same genotype. The next morning, females were checked for the presence of a vaginal plug, and then embryos

were isolated over several days using the morning of the plug as a reference (E0.5). To harvest embryos up to E2.5, oviducts were flushed, and for embryos between E3.0 and E4.0, uteruses were flushed in M2 media (Sigma Aldrich) in a petri dish. To locate the embryos, the plates were scanned under the microscope (10× lens). The identified embryos were transferred to a fresh drop of M2 media; images were captured with a camera-assisted Nikon microscope, followed by genotyping.

For genotyping, each embryo was washed in a drop of nuclease-free water and lysed in DNA lysis buffer. PCR reactions were carried out using three primers NDEL1: 5′-CAA TAG GAA TCC TAT GCC TGC TGA GG-3′; NDEL2: 5′-GTG GTG TGA AAA GAC ACA TGT CAG AGC-3′ and WT1: 5′-CCC TTG GAC CCA AGA GCA GAG CAG-3′. To see the position of the primer in the genomic allele of *Rpl13a*, please see Figure S1. PCR reactions using tail DNA from wild-type and *Rpl13a*+/− mice were used as reference. For wild-type embryos, one band of 599 bp is expected; for the heterozygous allele, two bands of 428 and 599 are expected; and for the KO allele, only one band of 428 is expected. For total RNA isolation, individual embryos (n = 25 embryos) from E3.0 were harvested from the intercross of *Rpl13a*+/− mice. Each embryo was washed in PBS and transferred to 10 μL of Cells-to-cDNA II Cell Lysis Buffer (Invitrogen Cat# AM8723), followed by lysis at 75°C for 10 min. For quantification of individual mRNAs, an aliquot of the lysate was subjected to genotyping to determine the +/+, +/−, and −/− embryos, and the remainder of the lysate was subjected to real-time PCR using a cDNA kit (Thermo fisher scientific Cat# 4374966) and Sybr Green Master Mix (Thermo fisher scientific Cat# A25741). For RNA sequencing, RNA isolation was performed from single embryos without genotyping using the PicoPure RNA isolation kit (Thermo fisher scientific, Cat#KIT0214) following the user's manual. RNA was eluted in 15 μL of elution buffer supplied in the kit. Note that after genotyping a single embryo, the remaining sample provided adequate quality and quantity of RNA for real-time PCR but not for RNA sequencing.

2.4 | RNA sequencing

Total RNA was normalized prior to oligo-dT capture and cDNA synthesis with Takara's SMART-Seq v4 Ultra Low Input RNA kits (mRNA). The resulting cDNA was assessed on the Fragment Analyzer with the High Sense Large Fragment kit and quantified using a Life Technologies' Qubit 3.0 fluorometer. Libraries were generated using Illumina's Nextera XT DNA Library Prep kit. High-depth sequencing (50 million reads per sample) was performed with an Illumina NextSeq 550 on a High Output, 75 base pairs, Paired End run. The data from the RNAseq are available on the NCBI Gene Expression Omnibus (GEO) site with an accession number of GSE 139241.

2.5 | Bioinformatics analysis

Raw demultiplexed fastq paired-end read files were trimmed of adapters and filtered using the program skewer[27] to cull any with an average paired quality score of <30 or a length of <36. Trimmed reads were then aligned using the HISAT2[28] aligner to the Mus Musculus NCBI reference genome assembly version GRCm38 and sorted using SAMtools.[29] Aligned reads were counted and assigned to gene meta-features using the program featurecounts[30] as part of the Subread package. These count files were imported

into the R programming language. They were assessed for quality control, normalized, and analyzed using an in-house pipeline utilizing the limma voom method[31] for regression analysis and the GSVA[32] library for gene set variation analysis. Quantile normalization was also applied during the voom transformation. The quantile normalized values of gene *Rpl13a* were used as the independent variable in limma's linear model framework to test for gene and pathways across samples that showed a significant statistical association with the KO phenotype. Ingenuity pathway analysis (Qiagen) and MSigDB collections (https://www.gsea-msigdb.org/gsea/msigdb/human/collections.jsp) were used as sources for pathway enrichment. Genes and pathways that did not show consistency between Pearson's correlation coefficient and linear coefficient of directionality were filtered out from the final results.

2.6 | Isolation of mouse preimplantation embryos for in vitro studies

CF-1 female mice 6–8 weeks of age were superovulated with 7.5 IU pregnant mare serum gonadotropin (ProsPec Bio, East Brunswick, NJ, USA), followed by 7.5 IU human chorionic gonadotropin (hCG) 48 h later (Millipore-Sigma, St. Louis, MO, USA). Superovulated females were then mated with B6D2F1 males, and one-cell embryos were collected from the oviducts at 20 h post-hCG injection. Oviducts were dissected to release one-cell embryos and cumulus cells were removed by repeated pipetting in M2 media containing hyaluronidase. Embryos were washed three times with M2 media and cultured in EmbryoMax® KSOM media (Millipore-Sigma) at 37°C in a humidified atmosphere containing 5% CO_2/5% O_2 balanced with N_2. All animal studies were carried out according to guidelines under currently approved protocols at Cleveland State University and Michigan State University.

2.7 | Microinjection of mouse preimplantation embryos

Microinjection was carried out as previously described.[33] Briefly, Injection micropipettes were pulled from micropipette tubes (Drummond, Birmingham, AL, USA) with a Narishige PC-10 puller (Narishige, Tokyo, Japan). The injection needle tip was cut to generate a 1–2 mM diameter opening. Microinjection was performed using a PL100 picoinjector (Harvard Apparatus, Holliston, MA, USA) mounted on an inverted laboratory microscope. Micromanipulation of one-cell embryos was performed in a manually prepared M2 medium. One-cell embryos were injected with 5–10 pL of 100 μM *Rpl13a* siRNA or 100 μM *Brg1* siRNA (SMART pool siRNA; Dharmacon, Lafayette, CO, USA), or control siRNA (ON-TARGETplus Non-Targeting Control siRNAs; Dharmacon) at 19–21 h post-hCG injection. After injection, embryos were cultured in KSOM media for 2–4 days, depending on the experiment.

2.8 | Quantitative real-time PCR (qRT-PCR) analysis of RPL13a knockdown embryos

Total mRNA was isolated from 20 to 30 embryos using the PicoPure RNA Isolation Kit (Arcturus, San Diego, CA, USA) according to the manufacturer's instructions. cDNA at each embryonic stage was synthesized using random hexamer and oligo(dT) primers and SuperScriptII reverse transcriptase (Invitrogen). qRT-PCR was performed using the TaqMan™ Universal PCR Master Mix and Taqman primer (ThermoFisher, Waltham, MA,

USA). Upstream-binding transcription factor (*Ubtf*) was used as a reference control. The gene-specific Taqman primers used in qRT-PCR are listed under the supplemental methods.

Quantification of snoRNAs was performed following the published methods[34–36]; embryos were injected with control and *Rpl13a* siRNA at the one-cell stage. Total RNAs were isolated from the morula stage (E3.25) using MagMAX™ mirVana™ total RNA isolation kit (applied biosystems Cat# A27828). cDNAs were synthesized using the snoRNA-specific stem-loop (SL) reverse transcription (RT) primer. qRT-PCR was performed using SYBR Green qPCR master mix and manually designed snoRNA-specific upstream primer and universal reverse primer based on a common sequence of the stem-loop primer. For qRT-PCR of snoRNAs, miR-16 was used as a reference control. For primer sequences, please see the supplementary methods.

2.9 | Immunofluorescent staining and in situ proximity ligation assay (PLA)

Embryos were fixed using 3.7% formaldehyde (Sigma-Aldrich) in PBS with 0.1% BSA for 20 min at room temperature. Next, embryos were permeabilized with 0.25% Triton X-100 in PBS for 30 min at room temperature. Embryos were blocked with PBS containing 3% BSA for 1 h at room temperature and incubated with primary antibodies in a blocking solution overnight at 4°C followed by incubation with Alexa Fluor 488 and 594 (Molecular Probes, Eugene, OR, USA) secondary antibodies for 30 min at room temperature. Finally, embryos were transferred to a blocking solution containing DAPI (4,6-diamidino-2-phenylindole; Vector Laboratories, Burlingame, CA, USA) for 10 min at room temperature. For the Duolink proximity ligation assay (PLA), embryos were fixed, permeabilized, and incubated with primary antibodies used for IF staining. Embryos were then incubated in PLA probes, followed by ligation, and amplification according to the manufacturer's protocol (Olink biosciences, Uppsala, Sweden). Images were acquired under an Olympus FluoView 1000 confocal microscope (CARV; Atto Bioscience, Rockville, MD, USA) with FluoView Viewer 3.0 software (Molecular Devices, Sunnyvale, CA, USA). Antibodies used for immunostaining were as follows: Rabbit anti-RPL13a (1:100; PA5-49192, Invitrogen, Burlington, ON, Canada) and mouse anti-BRG1 (1:100, SC-17796, Santa Cruz Biotechnology, Dallas, Texas, USA).

2.10 | Statistical analysis

Results are presented as mean ± SD. The statistical significance of the differences between groups was determined by a two-tailed Student's *t*-test. All statistical analysis was performed using GraphPad Prism 5.0 software.

3 | RESULTS

3.1 | Complete loss of RPL13a results in embryonic arrest during preimplantation development

Our previous studies involving myeloid-specific *Rpl13a* KO mice have demonstrated an important role of RPL13a in the endogenous mechanism of resolution of inflammation by macrophages. This mechanism relies on the translational control of target mRNAs (encoding a cohort of inflammatory proteins) mediated by the interaction of RPL13a, and

GAIT elements present in the 3′UTRs.[17–25] These fascinating findings motivated us to test the importance of this mechanism at the systemic level by creating an animal model of global RPL13a deficiency. To accomplish this, we created mice harboring a systemic heterozygous KO allele of *Rpl13a* (*Rpl13a*+/−) using a traditional gene targeting approach (see supplementary methods and Figure S1). When *Rpl13a*+/− females were crossed with *Rpl13a*+/− males, no pups containing the homozygous null allele were born, indicating *Rpl13a*−/− embryos are lethal during gestation (Figure S2A). We also observed 2.5 times greater number of *Rpl13a*+/− pups than *Rpl13a+/+* pups. To determine when *Rpl13a*−/− embryos die during gestation, we crossed *Rpl13a*+/− females, and *Rpl13a*+/− males and pregnant females were sacrificed at different time points between days 6.5 and 18.5 of gestation. Harvested embryos were microscopically inspected and then subjected to genotyping. Interestingly, only *Rpl13a+/+* and *Rpl13a*+/− embryos were identified during these developmental stages, and no apparent morphological defects were observed in those embryos. To determine if *Rpl13a*−/− embryos were implanted during early gestation and then died, we searched for resorption sites in pregnant *Rpl13a*+/− females. The uteri of *Rpl13a*+/− females did not show any resorption sites (Figure S2B), indicating that embryos harboring the homozygous *Rpl13a*, a null allele (*Rpl13a*−/−), could not successfully implant.

To further investigate the role of RPL13a in embryonic development and to pinpoint the specific stage of early lethality, we screened embryos during preimplantation development. Female and male *Rpl13a*+/− mice were crossed and embryos were collected at the two-cell (E1.5), morula (E3.0), and blastocyst stages (E4.0) from oviducts and uteri. The presence of *Rpl13a+/+*, +/− and −/− alleles at each stage was examined using PCR. A pair of bands with a size of 599 and 428 bp denote the presence of the +/− allele, and the presence of only one single band of 428 and 599 bp denotes the presence of −/− and +/+ alleles, respectively. A representative result from embryos genotyped at the two-cell, morula, and blastocyst stages is shown in Figure 1A. Morphological evaluation and genotyping at the two-cell and morula stages revealed the presence of morphologically normal-looking embryos with the representation of all three genotypes (Figure 1B). However, examination on E4.0 revealed the presence of only *Rpl13a+/+* and *Rpl13a*+/− blastocysts and no *Rpl13a*−/− blastocysts (Figure 1B). Beyond E4.0, we only observed lysed *Rpl13a*−/− embryo that did not hatch and implant. Altogether, these results show that *Rpl13a*−/− embryos can develop to the morula stage but arrest during the transition to the blastocyst stage.

3.2 | Morula harboring the homozygous null allele of *Rpl13a* (*Rpl13a−/−*) exhibit widespread alterations in gene expression and biological pathways

To gain further insights into the role of RPL13a during early embryogenesis, it is necessary to conduct a comprehensive analysis of the transcriptome. Because *Rpl13a*−/− embryos do not progress to the blastocyst stage, we focused our attention on morulae. Embryos were generated by crossing *Rpl13a*+/− mice and flushing the oviducts and uteri on E3.0. Individual embryos at the morula stage were evaluated under the microscope and then randomly selected for next-generation sequencing (NGS) without classical genotyping. According to our prior studies above, embryos at the morula stage harbored the wild-type, heterozygous, and homozygous null alleles of *Rpl13a*. A whole-transcriptome (mRNA) analysis was performed by ultra-low input RNAseq. Classical genotyping (e.g., PCR) of

single preimplantation stage embryos at E3.0 could not be performed because it did not leave enough biological material for the RNA sequencing-based studies to run in parallel. Instead, we used the transcriptome data to conduct a regression analysis and correlate bulk gene expression with each embryo's abundance of *Rpl13a* transcripts. Plots in Figure 2 show the top 50 positively (a) and negatively (b) correlating genes with Rpl*13a*. The linear regression coefficient estimates with 95% confidence intervals and is represented in the bar. The bar fill color represents Pearson's "*r*" value of the correlating genes, and the outline color of the bar designates their normal coefficient "*p*" value. Note that our knockout strategy did not target all introns and exons of the *Rpl13a* gene. Therefore, we could not identify any embryos in our regression analysis with absolute zero reads of *Rpl13a* transcripts. This type of observation is not unprecedented and was reported by others.[37] Nonetheless, our *Rpl13a*-based regression analysis revealed widespread alterations in gene expression that could be mined as a resource via biological pathway analysis. Figure 3 shows the ingenuity pathway enrichment analysis of the RNA seq data shows a strong and highly significant positive correlation with the regression scale of *Rpl13a* (*p* value ranging from .01 to .04). The data plot in Figure 3 shows that several pathways involved in the spliceosomal cycle, cellular metabolism, biosynthesis, and signaling are positively regulated with the extent of *Rpl13a* expression. This NGS-based analysis of the embryos also revealed a strong and highly significant (*p* value ranging from .01 to .04) negative correlation of several inflammatory pathways as defined by MSigDB Biocarta (Figure 4A), and a negative correlation of inflammatory molecules and intermediate molecules responsible for inflammatory signaling (Figure 4B). Together these studies provide some insights on why genetic depletion of *Rpl13a* may cause embryonic lethality during the morula-to-blastocyst transition. The data from the transcriptomic study are publicly available at the Gene Expression Omnibus (https://www.ncbi.nlm.nih.gov/geo) with an accession number of GSE 139241.

3.3 | Developmental expression and localization of RPL13a protein in preimplantation embryos and embryonic cells

To investigate the function of RPL13a during preimplantation development, we first evaluated its temporal and spatial expression. To accomplish this, we collected one-cell embryos from superovulated female mice and cultured them in vitro for up to 4 days. Confocal immunofluorescence analysis was conducted on embryos at the two-cell (E1.5), early morula (E3.25), and blastocyst stages (E4.5) using a RPL13a-specific antibody. In two-cell embryos and early morulae, RPL13a was detected in both the cytoplasm and nucleus (Figure 5A). However, at the blastocyst stage, RPL13a expression was decreased and was mainly localized to the cytoplasm and not detectable in the nucleus (Figure 5A). The specificity of the RPL13a antibody was confirmed using RPL13a knockdown (KD) embryos (shown in Figure 6A). To gain further insights into the expression of RPL13a in other embryonic cells, we examined the expression of RPL13a in mouse embryonic fibroblasts (MEFs) (Figure 5B). Consistent with the staining pattern of RPL13a in two-cell embryos and morulae, RPL13a was detected in both cytoplasmic and nuclear regions of MEFs. The nuclear to cytoplasm ratio was greater in MEFs compared to preimplantation embryos (Figure 5C). Collectively, these results show that *Rpl13a* has a unique expression

pattern and insinuates that nuclear RPL13a may have a potential role in the regulation of gene expression during preimplantation embryo development.

3.4 | RPL13a KD embryos phenocopy *Rpl13a* null embryos and exhibit decreased expression of lineage-specific genes

We employed RNA interference (RNAi) as a secondary approach for validating the *Rpl13a* null phenotype and investigating the role of RPL13a in blastocyst formation. To accomplish this, we injected either 100 μM *Rpl13a* siRNA or 100 μM control siRNA into one-cell embryos and placed them into in vitro culture for 4 days. Immunofluorescence analysis and qRT-PCR revealed a decrease in RPL13a protein and a 93.8% reduction in *Rpl13a* transcripts (Figure 6A,D). Embryo development was examined at the two-cell (E1.5), early morula (E3.25), and blastocyst stages (E4.5). Control and RPL13a KD embryos exhibited similar rates of development up to the morula stage. However, 78% of control embryos developed into blastocysts, whereas none of the RPL13a KD embryos progressed past the morula stage (Figure 6B; $p < .05$). Examination of control and RPL13a KD embryos on day 3.25 revealed that control and RPL13a KD morulae were morphologically similar (Figure 6C).

Because *Rpl13a* null and RPL13a KD embryos are arrested at the morula stage, we wanted to evaluate the expression of transcription factor genes required for normal blastocyst development. A key event during the morula to blastocyst transition is the establishment of the first two cellular lineages, the pluripotent inner cell mass (ICM) and the multipotent trophectoderm (TE). The ICM gives rise to the fetus and extra-embryonic yolk sac, while the TE forms the placenta. Therefore, we examined the expression of the ICM genes *Sox2* and *Pou5f1*, and TE gene *Cdx2* (Figure 6D). Embryos microinjected with either control siRNA or *Rpl13a* siRNA were cultured to the morula stage, and qRT-PCR was performed. In RPL13a KD embryos, *Sox2* and *Cdx2* were significantly reduced (93% and 79%), whereas *Pou5f1* levels were only moderately reduced (27%) (Figure 6D). Collectively, the above data demonstrate that RNAi-mediated depletion of RPL13a phenocopies the *Rpl13a* null phenotype and that key lineage genes required for blastocyst development are down-regulated.

3.5 | The observed developmental defects of *Rpl13a* deficient embryos are not due to the abrogation of the snoRNA genes harbored within the genomic locus of *Rpl13a*

snoRNA genes U32a, U33, and U34 are harbored within the intronic sequence of Rpl13a.[35,36] We tested whether the observed developmental defects of *Rpl13a*−/− embryos (Figure 1) are due to the abrogation of *Rpl13a* or are caused by consequential abrogation of the snoR-NAs. We took advantage of the fact that RNAi-mediated RPL13a knockdown also showed developmental arrest at the morula stage (Figure 6C), thus, phenocopying *Rpl13a* null embryos. Therefore, we tested the expression of U32a, U33, and U34 snoRNAs in RPL13a knockdown embryos and control embryos. Microinjections of control and *Rpl13a* siRNA were performed as described above. qRT-PCR was used to examine snoRNA and RPL13a expression in RPL13a KD and control embryos (Figure 7A,B). These results revealed that RNAi-mediated knockdown of RPL13a did not abrogate the expression of the snoRNAs U32a, U33, and U34. This result is also consistent with the fact that RNAi

is mostly a cytoplasmic event. The RNA-degrading RISC complex forms in the cytoplasm and, in general, does not target intron-containing pre-mRNA in the nucleus.[38] These results indicate that RPL13a itself is required for blastocyst formation.

3.6 | Genetic and RNAi-mediated abrogation of *Rpl13a* during preimplantation development causes increased expression of *IL-7* and *IL-17*

Based on the inflammatory pathway analysis in Figure 3 and our previous findings in myeloid-specific *Rpl13a* KO mice,[20–23] we wanted to evaluate the *IL-7* and *IL-17* expression in embryos harboring wild-type and homozygous null alleles of *Rpl13a*. To accomplish this, embryos at the morula stage were genotyped (data not shown), followed by qRT-PCR using primers for *Rpl13a*, *IL-7*, and *IL-17*. Consistent with inflammatory pathway analysis, we observed increased expression of *IL-7* and *IL-17* in *Rpl13a*−/− embryos compared to wild-type embryos, and as expected, *Rpl13a* transcripts were not detectable in *Rpl13a*−/− embryos (Figure 8A). As a complementary approach, we microinjected *Rpl13a* siRNA into one-cell embryos and cultured them to the morula stage. Like the knockout phenotype, both *IL-7* and *IL-17* expressions were upregulated in RPL13a KD embryos (Figure 8B). These data suggest that RPL13a may play a conserved role in repressing a subset of key inflammatory genes in preimplantation embryos. Currently, we do not know whether RPL13a represses these genes via translational control or direct transcriptional or posttranscriptional regulation. Our current data will serve as a foundation for future mechanistic studies.

3.7 | RPL13a is associated with chromatin proteins during preimplantation development

Most ribosomal proteins are involved in maintaining the optimum ribosomal function of protein synthesis in the cytoplasm.[39,40] The observed nuclear localization of RPL13a in early embryos indicates a potential extraribosomal function in gene transcription. However, it is not known whether RPL13a is associated with chromatin during early embryogenesis. Previous studies using high-resolution LC–MS/MS spectrometry in WiT49 cells and human lung cancer cells revealed brahma-related gene 1 (BRG1) as a component of the SWI/SNF chromatin remodeling complex for the activation and repression of transcription.[41] BRG1 is also indispensable for early embryonic development, with roles in genomic imprinting and transcriptional regulation.[42,43] Considering the importance of BRG1 in early development, we speculated that RPL13a might form a complex with this chromatin-associated protein during early embryogenesis.

To determine whether RPL13a interacts with BRG1 during preimplantation development, we performed a Duolink proximity ligation assay (PLA). PLA is a fluorescence-based method for in situ detection of protein–protein interactions. We evaluated interactions in eight-cell embryos (E2.5) and early morulae (E3.25) because RP13a was localized in the nucleus at these stages. Accordingly, we found that BRG1 and RPL13a interact in eight-cell embryos and morulae, as detected by a strong red fluorescence signal (Figure 9A). To confirm whether this signal was generated by interactions between RPL13a and BRG1, we carried out PLA analysis in BRG1 KD embryos. Microinjection of *Brg1* siRNA caused an 89.7% decrease in *Brg1* transcripts (Figure 9B) and a corresponding decrease in BRG1 protein (data not shown). PLA analysis in BRG1 KD embryos resulted in a significant loss

of PLA signal (Figure 9A), demonstrating that RPL13a-BRG1 interaction is specific. In this context, it is possible that the interaction of the ribosomal protein with chromatin protein within the nucleus might not be exclusive to RPL13a. Through additional PLA analysis, we found that RPL26 also associates with BRG1 during preimplantation development (Figure S3). Collectively, these data implicate the association of RPL13a with chromatin. However, mechanistic insights into the role of RPL13a in regulating gene expression at the transcriptional level require further investigation.

4 | DISCUSSION

The protein synthesis machinery and a few individual ribosomal proteins play a critical role in the more mature stages of embryonic development.[5,7–11] However, the roles of these components during early embryonic development remain unclear. Using a mouse model, we report that RPL13a is required for preimplantation embryo development.

Our motivation to create a systemic KO of *Rpl13a* is based on the results of two previous studies from our laboratory. First, RNAi-mediated KD of RPL13a did not compromise protein synthesis activity of ribosome and survival of the KD cells[16] and secondly, Myeloid-specific *Rpl13a* KO mice are viable and demonstrate the physiological role of RPL13a and GAIT-element mediated translational silencing as a mechanism to control inflammation.[20–25] However, in contrast to our expectation, no *Rpl13a*−/− pups were born after crossing heterozygous *Rpl13a*+/− mice, and we found no *Rpl13a*−/− embryos or any resorption sites in the uterus between E6.5 and E18.5. These results lead us to hypothesize that the embryonic lethality caused by the presence of *Rpl13a* homozygous null allele occurred during the window of preimplantation embryo development. Consistent with this hypothesis, we found that the *Rpl13a* null allele was able to develop up to the morula stage (E3.5) but then became lethal upon transition to the blastocyst stage (E4.5). Importantly, RPL13a KD embryos phenocopied *Rpl13a*−/− embryos and arrested at the morula stage. We cannot completely rule out that RPL13a is not required prior to the morula stage because residual maternal protein provided by the oocyte may have masked an earlier phenotype. Nevertheless, these results strongly demonstrate that zygotic RPL13a is required for blastocyst formation.

The morula-specific lethality caused by the presence of the *Rpl13a* homozygous null allele prompted us to investigate the effects on global gene expression by NGS. We found highly significant differential gene expression with reference to the regression scale of *Rpl13a*, thus showing RPL13a-associated increases and decreases in a large dataset of genes and pathways at the morula stage, a resource we have uploaded publicly as GEO accession #GSE139241. It is important to note that we found differential expression of many critical genes showing negative and positive correlations with the expression of *Rpl13a*. These results included but were not limited to *Zbed* 3, which regulates β catenin signaling[44] and division of blastomeres in early embryogenesis,[45] *Tcl1b* that activates serine/threonine kinase,[46] *Omt2b* an oocyte maturation factor,[47] *Klf17* a germ cell-specific transcription factor,[48] *Rnf113a2* a splicing factor and component of spliceosome,[49] *Stam* which has a role in endosomal sorting complex formation,[50] *Gpx2* a regulator of epithelial-mesenchymal transition[51] and redox signaling,[52] *Rab39* a stemness factor,[53] *Cadm1*, an

adhesion molecule, and cell survival factor,[54] *Pfkfb2* a regulator of glycolysis,[55] and *Cbx7* a molecule that regulates pluripotency[56] and cell migration.[57] The ingenuity pathway enrichment analysis showed a strong positive correlation between many fundamental cellular pathways with *Rpl13a* expression. Notably, pathways involving the spliceosomal cycle and several amino acid metabolism pathways are among them. These results are consistent with the possibility that *Rpl13a*−/− morulae die upon transition to the blastocyst stage due to compromised gene expression caused by disruption of critical transcription factor networks, splicing of essential transcripts, and/or synthesis of amino acids.

Another intriguing aspect of RNA seq data is the activation of several pathways regulating cytokine synthesis, and many genes involved in inflammatory response show a significant negative correlation with the regression scale of *Rpl13a*. qRT-PCR analysis in both *Rpl13a* null and RPL13a KD embryos confirmed that *IL-7* and *IL-17* expression was increased at the morula stage. Interestingly, these findings are consistent with our previous results using macrophage-specific *Rpl13a* KO mice. These mice show the physiological activation of inflammatory response in the absence of RPL13a in myeloid cells.[21–25] A few studies have looked at the relationship between inflammation and pluripotency[58,59] however, myeloid cells develop from yolk sac hematopoiesis from embryonic day E8.5 which is several days after implantation.[60,61] At this stage of the investigation, it remains unclear how inflammation could initiate in the total absence of myeloid cells at the preimplantation stages. An earlier study demonstrated that several inflammatory genes and their receptors are expressed in mouse preimplantation embryos,[62,63] and it is established that proinflammatory cytokines are important for blastocyst implantation.[64–66] Thus, RPL13a may function as part of a repressive mechanism to control the expression of proinflammatory cytokines prior to blastocyst implantation. In this context, the altered gene expression in RPL13a KO and KD embryos observed through bulk RNA sequencing and real-time PCR may not confirm a direct transcriptional role of this ribosomal protein. These methods only measure the steady state level of mRNAs. Thus, the impact on gene expression could be indirect. For example, RPL13a may target essential transcriptional factors or, by virtue of its RNA-binding properties,[18,20,67] target expressed pre-mRNA in the nucleus, thus altering its steady-state level. Detailed follow-up studies involving RNA-immunoprecipitation-based sequencing (RIP-seq) and chromatin-immunoprecipitation-based sequencing (ChIP-seq) will be essential to address this issue.

The presence of snoRNAs U32a, U33, and U34 in the *Rpl13a* genomic locus[35,36] raises the possibility that defect in embryonic development may originate from the loss of these snoRNAs in *Rpl13a*−/− embryos. However, RPL13a knockdown embryos exhibited the same developmental defect as *Rpl13a*−/− embryos without the abrogation of these snoRNAs (Figure 7), arguing against that logic. However, even though RNAi-mediated knockdown of RPL13a did not disrupt the snoRNAs harbored in the *Rpl13a* pre-mRNAs, we cannot completely rule out the potential effects of altered snoRNAs on gene expression in our *Rpl13a*−/− embryo RNA seq dataset.

The role of ribosomal proteins in embryonic development is not unprecedented. For proteins from the large ribosomal subunit, embryonic lethality was observed for *RPL11* heterozygous embryos,[68] *Rpl7l1* knockdown embryos,[69,70] and RPL14, RPL18, and RPL23

were identified as the regulators of the two-cell stage transcriptome in mouse embryonic stem cells.[71] For proteins from the small ribosomal subunit, mice homozygous for the disrupted RPS19 were found to be lethal prior to implantation,[72] and haploinsufficiency of RPS6 gene is lethal at embryonic day 5.5.[73] RPL13a is a ribosomal protein of the large subunit, and the site for ribosome synthesis occurs in the nucleolus, a specialized compartment of the nucleus. However, previous studies also show that the boundary between the nucleolus and the rest of the nucleus is dynamic, and many nucleolar proteins involved in ribosome biogenesis also cycle between the nucleolus, nucleoplasm, and chromosome.[74–76] Therefore, it is expected that some RPL13a engaged in the flux of ribosome biogenesis will be in the nucleus. Genome activation begins between the one-cell and two-cell stages and requires transcriptional activation as well as protein synthesis activity mediated by ribosome synthesis.[77] Our earlier work using myeloid cells showed that RPL13a might not be required for the protein synthesis activity and biogenesis of the ribosome.[16] These data are consistent with the survival of homozygous *Rpl13a* null (Figure 1B) and RPL13a KD embryos (Figure 6C) up to the morula stage. However, at the same time, we are also open to the possibility that during early embryonic development, RPL13a may have a role in global protein synthesis, ribosome biogenesis and the potential contribution of the maternal remnant protein.

Future studies in preimplantation embryos and embryonic stem cells are required to determine the precise mechanism by which RPL13a regulates gene expression during morula-to-blastocyst transition in mice.

Supplementary Material

Refer to Web version on PubMed Central for supplementary material.

ACKNOWLEDGMENTS

This work was supported by the National Institutes of Health (NIH) grants HL79164 (to B.M.) and HD095371 (to J.G.K), MSU AgBioResearch and by the Cleveland State University Office of Research, and the Center for Gene Regulation in Health and Disease. We thank members of the CWRU Applied Functional Genomics Core for their support of the RNAseq assays.

Funding information

AgBioResearch, Michigan State University (MSU AgBioResearch); Center for Gene Regulation in Health and Disease Cleveland State University; HHS | NIH | Eunice Kennedy Shriver National Institute of Child Health and Human Development (NICHD), Grant/Award Number: HD095371; HHS | NIH | National Heart, Lung, and Blood Institute (NHLBI), Grant/Award Number: HL79164; Office of Research Cleveland State University

DATA AVAILABILITY STATEMENT

Data obtained from bulk RNA sequences of mouse embryos are available on the NCBI Gene Expression Omnibus (GEO) site. The accession number for this data is GSE 139241. These data are available from the link https://www.ncbi.nlm.nih.gov/geo/query/acc.cgi?acc=GSE139241.

Abbreviations:

BRG1	brahma-related-gene1
Cdx2	caudal type homeobox 2
ChIP	chromatin immunoprecipitation
DAPI	4,6-diamidino-2-phenylindole
DSS	dextran sodium sulfate
E	embryonic day
GEO	gene expression omnibus
GSVA	gene set variation analysis
HCG	human chorionic gonadotropin
HFD	high-fat diet
ICM	inner cell mass
IFN-γ	interferon-gamma
IL-17	interleukin 17
IL-7	interleukin 7
KD	knockdown
KO	knockout
LPS	lipopolysaccharide
MEF	mouse embryonic fibroblast
NCBI	National Center for Biotechnology Information
NGS	next-generation-sequencing
PLA	proximity ligation assay
PMSG	pregnant mare serum gonadotropin
Pou5f1	POU class 5 homeobox 1
qRT-PCR	quantitative real-time PCR
RIP	RNA-immunoprecipitation
RPL13a	ribosomal protein L13a
SD	standard deviation
snoRNA	small nucleolar RNA

Sox2	SRY (sex determining region Y)-box 2
TE	trophectoderm
Ubtf	upstream-binding transcription factor
UTR	untranslated region

REFERENCES

1. Karasek C, Ashry M, Driscoll CS, Knott JG. A tale of two cell-fates: role of the hippo signaling pathway and transcription factors in early lineage formation in mouse preimplantation embryos. Mol Hum Reprod. 2020;26(9):653–664. [PubMed: 32647873]
2. Hamatani T, Carter MG, Sharov AA, Ko MS. Dynamics of global gene expression changes during mouse preimplantation development. Dev Cell. 2004;6(1):117–131. [PubMed: 14723852]
3. Gao Y, Liu X, Tang B, et al. Protein expression landscape of mouse embryos during preimplantation development. Cell Rep. 2017;21(13):3957–3969. [PubMed: 29281840]
4. Xue Z, Huang K, Cai C, et al. Genetic programs in human and mouse early embryos revealed by single-cell RNA sequencing. Nature. 2013;500(7464):593–597. [PubMed: 23892778]
5. Topisirovic I, Sonenberg N. Translational control by the eukaryotic ribosome. Cell. 2011;45(3):333–334.
6. Karp GC, Manes C, Hahn WE. Ribosome production and protein synthesis in the preimplantation rabbit embryo. Differentiation. 1974;2(2):65–73. [PubMed: 4479837]
7. Chau KF, Shannon ML, Fame RM, et al. Downregulation of ribosome biogenesis during early forebrain development. eLife. 2018;7:e36998. [PubMed: 29745900]
8. Sanchez CG, Teixeira FK, Czech B, et al. Regulation of ribosome biogenesis and protein synthesis controls germline stem cell differentiation. Cell Stem Cell. 2016;18(2):276–290. [PubMed: 26669894]
9. Fujii K, Shi Z, Zhulyn O, Denans N, Barna M. Pervasive translational regulation of the cell signalling circuitry underlies mammalian development. Nat Commun. 2017;8:14443. [PubMed: 28195124]
10. Kondrashov N, Pusic A, Stumpf CR, et al. Ribosome-mediated specificity in hox mRNA translation and vertebrate tissue patterning. Cell. 2011;145(3):383–397. [PubMed: 21529712]
11. Perucho L, Artero-Castro A, Guerrero S, et al. Rplp1, a crucial ribosomal protein for embryonic development of the nervous system. PLoS ONE. 2014;9(6):e99956. [PubMed: 24959908]
12. Narla A, Ebert BL. Ribosomopathies: human disorders of ribosome dysfunction. Blood. 2010;115(16):3196–3205. [PubMed: 20194897]
13. Wang W, Nag S, Zhang X, et al. Ribosomal proteins and human diseases: pathogenesis, molecular mechanisms, and therapeutic implications. Med Res Rev. 2015;35(2):225–285. [PubMed: 25164622]
14. Anderson SJ, Lauritsen JP, Hartman MG, et al. Ablation of ribosomal protein l22 selectively impairs alphabeta T cell development by activation of a p53-dependent checkpoint. Immunity. 2007;26(6):759–772. [PubMed: 17555992]
15. Alexander SJ, Woodling NS, Yedvobnick B. Insertional inactivation of the l13a ribosomal protein gene of drosophila melanogaster identifies a new minute locus. Gene. 2006;368:46–52. [PubMed: 16326033]
16. Chaudhuri S, Vyas K, Kapasi P, et al. Human ribosomal protein l13a is dispensable for canonical ribosome function but indispensable for efficient rRNA methylation. RNA. 2007;13(12):2224–2237. [PubMed: 17921318]
17. Vyas K, Chaudhuri S, Leaman DW, et al. Genome-wide polysome profiling reveals an inflammation-responsive posttranscriptional operon in gamma interferon-activated monocytes. Mol Cell Biol. 2009;29(2):458–470. [PubMed: 19001086]

18. Mazumder B, Sampath P, Seshadri V, Maitra RK, DiCorleto PE, Fox PL. Regulated release of l13a from the 60s ribosomal subunit as a mechanism of transcript-specific translational control. Cell. 2003;115(2):187–198. [PubMed: 14567916]
19. Sampath P, Mazumder B, Seshadri V, et al. Noncanonical function of glutamyl-prolyl-tRNA synthetase: gene-specific silencing of translation. Cell. 2004;119(2):195–208. [PubMed: 15479637]
20. Basu A, Jain N, Tolbert BS, Komar AA, Mazumder B. Conserved structures formed by heterogeneous RNA sequences drive silencing of an inflammation responsive post-transcriptional operon. Nucleic Acids Res. 2017;45(22):12987–13003. [PubMed: 29069516]
21. Poddar D, Basu A, Baldwin WM 3rd, Kondratov RV, Barik S, Mazumder B. An extraribosomal function of ribosomal protein l13a in macrophages resolves inflammation. J Immunol. 2013;190(7):3600–3612. [PubMed: 23460747]
22. Basu A, Poddar D, Robinet P, et al. Ribosomal protein l13a deficiency in macrophages promotes atherosclerosis by limiting translation control-dependent retardation of inflammation. Arterioscler Thromb Vasc Biol. 2014;34(3):533–542. [PubMed: 24436370]
23. Basu A, Dvorina N, Baldwin WM 3rd, Mazumder B. High-fat diet-induced gait element-mediated translational silencing of mRNAs encoding inflammatory proteins in macrophage protects against atherosclerosis. FASEB J. 2020;34(5):6888–6906. [PubMed: 32232901]
24. Poddar D, Kaur R, Baldwin WM 3rd, Mazumder B. L13a-dependent translational control in macrophages limits the pathogenesis of colitis. Cell Mol Immunol. 2016;13(6):816–827. [PubMed: 26166763]
25. Mazumder B Gaiting the gut. Cell Mol Immunol. 2018;15:1082–1084. [PubMed: 29769660]
26. Carey TS, Cao Z, Choi I, et al. Brg1 governs nanog transcription in early mouse embryos and embryonic stem cells via antagonism of histone h3 lysine 9/14 acetylation. Mol Cell Biol. 2015;35(24):4158–4169. [PubMed: 26416882]
27. Jiang H, Lei R, Ding SW, Zhu S. Skewer: a fast and accurate adapter trimmer for next-generation sequencing paired-end reads. BMC Bioinform. 2014;15:182.
28. Zhang Y, Park C, Bennett C, Thornton M, Kim D. Rapid and accurate alignment of nucleotide conversion sequencing reads with HISAT-3N. Genome Res. 2021;31:1290–1295. doi:10.1101/gr.275193.120 [PubMed: 34103331]
29. Li H, Handsaker B, Wysoker A, et al. The sequence alignment/map format and samtools. Bioinformatics. 2009;25(16):2078–2079. [PubMed: 19505943]
30. Liao Y, Smyth GK, Shi W. Featurecounts: an efficient general purpose program for assigning sequence reads to genomic features. Bioinformatics. 2014;30(7):923–930. [PubMed: 24227677]
31. Ritchie ME, Phipson B, Wu D, et al. Limma powers differential expression analyses for RNA-sequencing and microarray studies. Nucleic Acids Res. 2015;43(7):e47. [PubMed: 25605792]
32. Hanzelmann S, Castelo R, Guinney J. GSVA: gene set variation analysis for microarray and RNA-seq data. BMC Bioinform. 2013;14:7.
33. Choi I, Carey TS, Wilson CA, Knott JG. Transcription factor ap2gamma is a core regulator of tight junction biogenesis and cavity formation during mouse early embryogenesis. Development. 2012;139(24):4623–4632. [PubMed: 23136388]
34. Kramer MF. Stem-loop RT-qPCR for miRNAs. Curr Protoc Mol Biol. 2011;95:10–15. doi:10.1002/0471142727.mb1510s95
35. Lee J, Harris AN, Holley CL, et al. Rpl13a small nucleolar RNAs regulate systemic glucose metabolism. J Clin Invest. 2016;126(12):4616–4625. [PubMed: 27820699]
36. Michel CI, Holley CL, Scruggs BS, et al. Small nucleolar RNAs u32a, u33, and u35a are critical mediators of metabolic stress. Cell Metab. 2011;14(1):33–44. [PubMed: 21723502]
37. Han Y-H, Mao Y-Y, Yu N-N, et al. RNA sequencing reveals that *Prx II* gene knockout can down-regulate the allograft rejection of dermal mesenchymal stem cells. Appl Biol Chem. 2020;63:30. doi:10.1186/s13765-020-00515-z
38. Dykxhoorn DM, Novina CD, Sharp PA. Killing the messenger: short RNAs that silence gene expression. Nat Rev Mol Cell Biol. 2003;4(6):457–467. [PubMed: 12778125]
39. Warner JR, McIntosh KB. How common are extraribosomal functions of ribosomal proteins? Mol Cell. 2009;34(1):3–11. [PubMed: 19362532]

40. Zhou X, Liao WJ, Liao JM, Liao P, Lu H. Ribosomal proteins: functions beyond the ribosome. J Mol Cell Biol. 2015;7(2):92–104. [PubMed: 25735597]
41. Marino MM, Rega C, Russo R, et al. Interactome mapping defines brg1, a component of the swi/snf chromatin remodeling complex, as a new partner of the transcriptional regulator ctcf. J Biol Chem. 2019;294(3):861–873. [PubMed: 30459231]
42. Bultman S, Gebuhr T, Yee D, et al. A brg1 null mutation in the mouse reveals functional differences among mammalian swi/snf complexes. Mol Cell. 2000;6(6):1287–1295. [PubMed: 11163203]
43. Kidder BL, Palmer S, Knott JG. Swi/snf-brg1 regulates self-renewal and occupies core pluripotency-related genes in embryonic stem cells. Stem Cells. 2009;27(2):317–328. [PubMed: 19056910]
44. Chen T, Li M, Ding Y, et al. Identification of zinc-finger bed domain-containing 3 (zbed3) as a novel axin-interacting protein that activates wnt/beta-catenin signaling. J Biol Chem. 2009;284(11):6683–6689. [PubMed: 19141611]
45. Gao Z, Zhang X, Yu X, et al. Zbed3 participates in the subcortical maternal complex and regulates the distribution of organelles. J Mol Cell Biol. 2018;10(1):74–88. [PubMed: 28992324]
46. Laine J, Kunstle G, Obata T, Sha M, Noguchi M. The protooncogene tcl1 is an akt kinase coactivator. Mol Cell. 2000;6(2):395–407. [PubMed: 10983986]
47. West MF, Verrotti AC, Salles FJ, Tsirka SE, Strickland S. Isolation and characterization of two novel, cytoplasmically polyadenylated, oocyte-specific, mouse maternal RNAs. Dev Biol. 1996;175(1):132–141. [PubMed: 8608859]
48. van Vliet J, Crofts LA, Quinlan KG, Czolij R, Perkins AC, Crossley M. Human klf17 is a new member of the sp/klf family of transcription factors. Genomics. 2006;87(4):474–482. [PubMed: 16460907]
49. Zhang X, Yan C, Zhan X, Li L, Lei J, Shi Y. Structure of the human activated spliceosome in three conformational states. Cell Res. 2018;28(3):307–322. [PubMed: 29360106]
50. Gruenberg J, Stenmark H. The biogenesis of multivesicular endosomes. Nat Rev Mol Cell Biol. 2004;5(4):317–323. [PubMed: 15071556]
51. Li F, Dai L, Niu J. Gpx2 silencing relieves epithelial-mesenchymal transition, invasion, and metastasis in pancreatic cancer by downregulating wnt pathway. J Cell Physiol. 2020;235(11):7780–7790. [PubMed: 31774184]
52. Ren Z, Liang H, Galbo PM Jr, et al. Redox signaling by glutathione peroxidase 2 links vascular modulation to metabolic plasticity of breast cancer. Proc Natl Acad Sci U S A. 2022;119(8):e2107266119. [PubMed: 35193955]
53. Chano T, Avnet S. Rab39a: a rab small GTPase with a prominent role in cancer stemness. J Biochem. 2018;164(1):9–14. [PubMed: 29648608]
54. Hagiyama M, Kimura R, Yoneshige A, Inoue T, Otani T, Ito A. Cell adhesion molecule 1 contributes to cell survival in crowded epithelial monolayers. Int J Mol Sci. 2020;21(11):4123. [PubMed: 32527032]
55. Ozcan SC, Sarioglu A, Altunok TH, et al. Pfkfb2 regulates glycolysis and proliferation in pancreatic cancer cells. Mol Cell Biochem. 2020;470(1–2):115–129. [PubMed: 32415418]
56. Fan JR, Lee HT, Lee W, et al. Potential role of CBX7 in regulating pluripotency of adult human pluripotent-like olfactory stem cells in stroke model. Cell Death Dis. 2018;9(5):502. [PubMed: 29717132]
57. Bao Z, Xu X, Liu Y, et al. Cbx7 negatively regulates migration and invasion in glioma via wnt/beta-catenin pathway inactivation. Oncotarget. 2017;8(24):39048–39063. [PubMed: 28388562]
58. Lee J, Sayed N, Hunter A, et al. Activation of innate immunity is required for efficient nuclear reprogramming. Cell. 2012;151(3):547–558. [PubMed: 23101625]
59. O'Neill LA. "Transflammation": when innate immunity meets induced pluripotency. Cell. 2012;151(3):471–473. [PubMed: 23101619]
60. Ginhoux F, Jung S. Monocytes and macrophages: developmental pathways and tissue homeostasis. Nat Rev Immunol. 2014;14(6):392–404. [PubMed: 24854589]
61. Stremmel C, Schuchert R, Wagner F, et al. Yolk sac macrophage progenitors traffic to the embryo during defined stages of development. Nat Commun. 2018;9(1):75. [PubMed: 29311541]

62. Basak S, Dubanchet S, Zourbas S, Chaouat G, Das C. Expression of pro-inflammatory cytokines in mouse blastocysts during implantation: modulation by steroid hormones. Am J Reprod Immunol. 2002;47(1):2–11. [PubMed: 11883745]

63. Gerwin N, Jia GQ, Kulbacki R, Gutierrez-Ramos JC. Interleukin gene expression in mouse preimplantation development. Dev Immunol. 1995;4(3):169–179. [PubMed: 8770556]

64. Dekel N, Gnainsky Y, Granot I, Mor G. Inflammation and implantation. Am J Reprod Immunol. 2010;63(1):17–21. [PubMed: 20059465]

65. Seshagiri PB, Vani V, Madhulika P. Cytokines and blastocyst hatching. Am J Reprod Immunol. 2016;75(3):208–217. [PubMed: 26706391]

66. Griffith OW, Chavan AR, Protopapas S, Maziarz J, Romero R, Wagner GP. Embryo implantation evolved from an ancestral inflammatory attachment reaction. Proc Natl Acad Sci U S A. 2017;114(32):e6566–e6575. [PubMed: 28747528]

67. Sampath P, Mazumder B, Seshadri V, Fox PL. Transcript-selective translational silencing by gamma interferon is directed by a novel structural element in the ceruloplasmin mRNA 3′ untranslated region. Mol Cell Biol. 2003;23(5):1509–1519. [PubMed: 12588972]

68. Morgado-Palacin L, Varetti G, Llanos S, Gomez-Lopez G, Martinez D, Serrano M. Partial loss of *Rpl11* in adult mice recapitulates diamond-blackfan anemia and promotes lymphomagenesis. Cell Rep. 2015;13:712–722. [PubMed: 26489471]

69. Maserati M, Dai X, Walentuk M, Mager J. Identification of four genes required for mammalian blastocyst formation. Zygote. 2014;22(3):331–339. [PubMed: 23211737]

70. Cui W, Dai X, Marcho C, et al. Towards functional annotation of the preimplantation transcriptome: an RNAi screen in mammalian embryos. Sci Rep. 2016;6:37396. [PubMed: 27869233]

71. Yi Y, Zeng Y, Sam TW, et al. Ribosomal proteins regulate 2-cell-stage transcriptome in mouse embryonic stem cells. Stem Cell Rep. 2023;18:463–474.

72. Matsson H, Davey EJ, Draptchinskaia N, et al. Targeted disruption of the ribosomal protein S19 gene is lethal prior to implantation. Mol Cell Biol. 2004;24(9):4032–4037. [PubMed: 15082795]

73. Panic L, Tamarut S, Sticker-Jantscheff M, et al. Ribosomal protein S6 gene haploinsufficiency is associated with activation of a p53-dependent checkpoint during gastrulation. Mol Cell Biol. 2006;26(23):8880–8891. [PubMed: 17000767]

74. Boisvert FM, van Koningsbruggen S, Navascues J, Lamond AI. The multifunctional nucleolus. Nat Rev Mol Cell Biol. 2007;8(7):574–585. [PubMed: 17519961]

75. Chen D, Huang S. Nucleolar components involved in ribosome biogenesis cycle between the nucleolus and nucleoplasm in interphase cells. J Cell Biol. 2001;153:169–176. [PubMed: 11285283]

76. Ma N, Matsunaga S, Takata H, Ona-Maniwa R, Uchiyama S, Fukui K. Nucleolin functions in nucleolus formation and chromosome congression. J Cell Sci. 2007;120:2091–2105. [PubMed: 17535846]

77. Wang Q, Chung YG, deVries WN, Struwe M, Latham KE. Role of protein synthesis in the development of a transcriptionally permissive state in one-cell stage mouse embryos. Biol Reprod. 2001;65(3):748–754. [PubMed: 11514337]

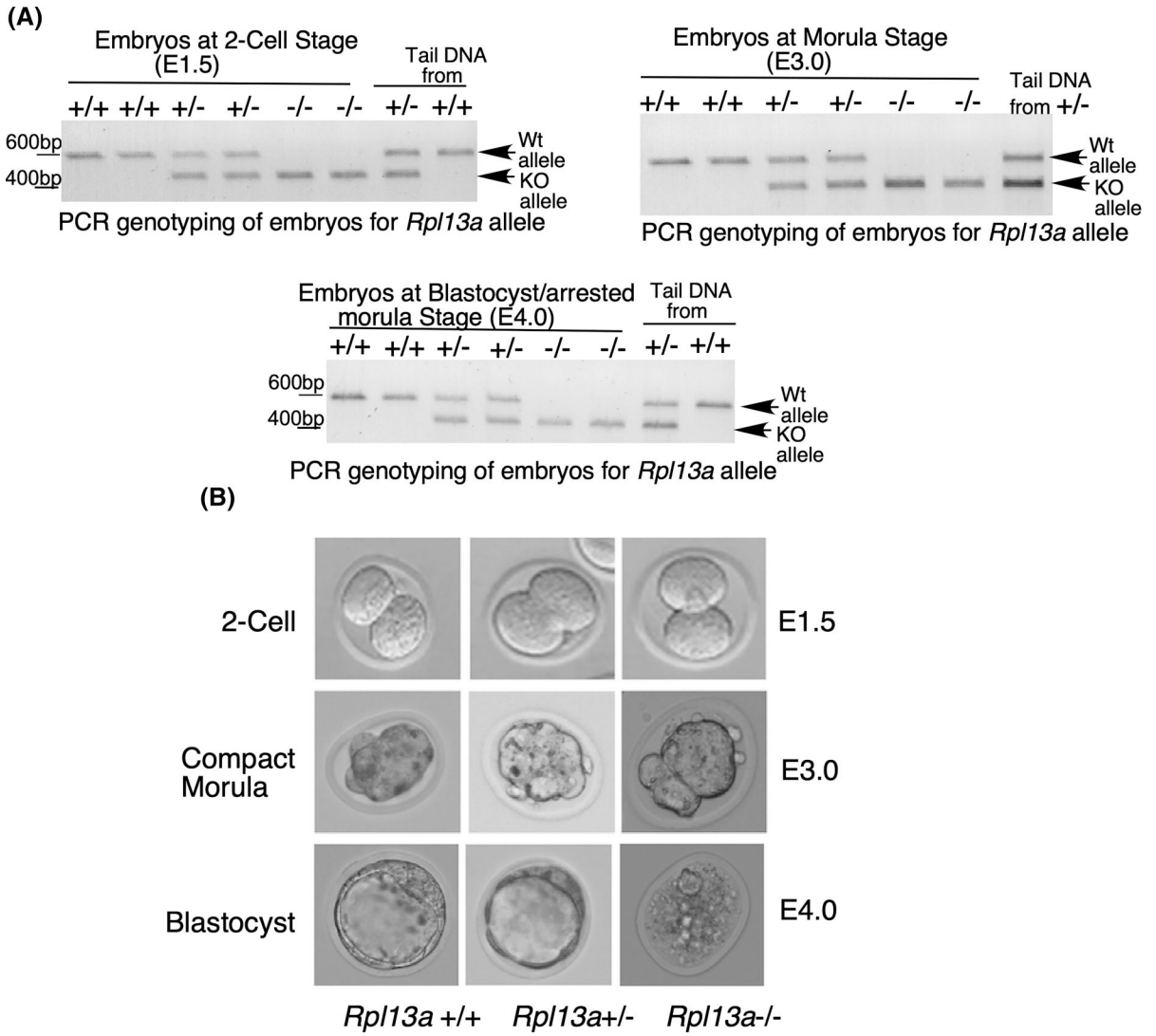

FIGURE 1.

Embryos with the *Rpl13a* null allele arrest at the morula stage. (A) PCR genotyping of mouse preimplantation embryos to detect the *Rpl13a* KO allele. Preimplantation embryos at the two-cell (E1.5), morula (E3.0), and blastocysts (E4.0), generated from the cross between the mice harboring the heterozygous null allele of *Rpl13a* were subjected to PCR genotyping with specific primers. Embryos harboring the wild-type allele and the homozygous and heterozygous KO allele for *Rpl13a* are shown. PCR reactions using tail DNA from wild-type and heterozygous mice were used as references. (B) Embryos were harvested after flushing the oviduct to collect two-cell, morula, and blastocysts, respectively. Embryos were collected by a capillary pipette and mounted on the center of the glass slide on a drop of PBS. Morphological images were captured by camera assisted Nikon microscope (10× lens). The embryos were lysed, and the wild-type, homozygous, and heterozygous null alleles of *Rpl13a* were detected by PCR. *Rpl13a*+/+ and +/− embryos were identified at the two-cell,

morula, and blastocyst stages. However, embryos with homozygous KO allele of *Rpl13a* only developed to the morula stage and failed to produce blastocysts.

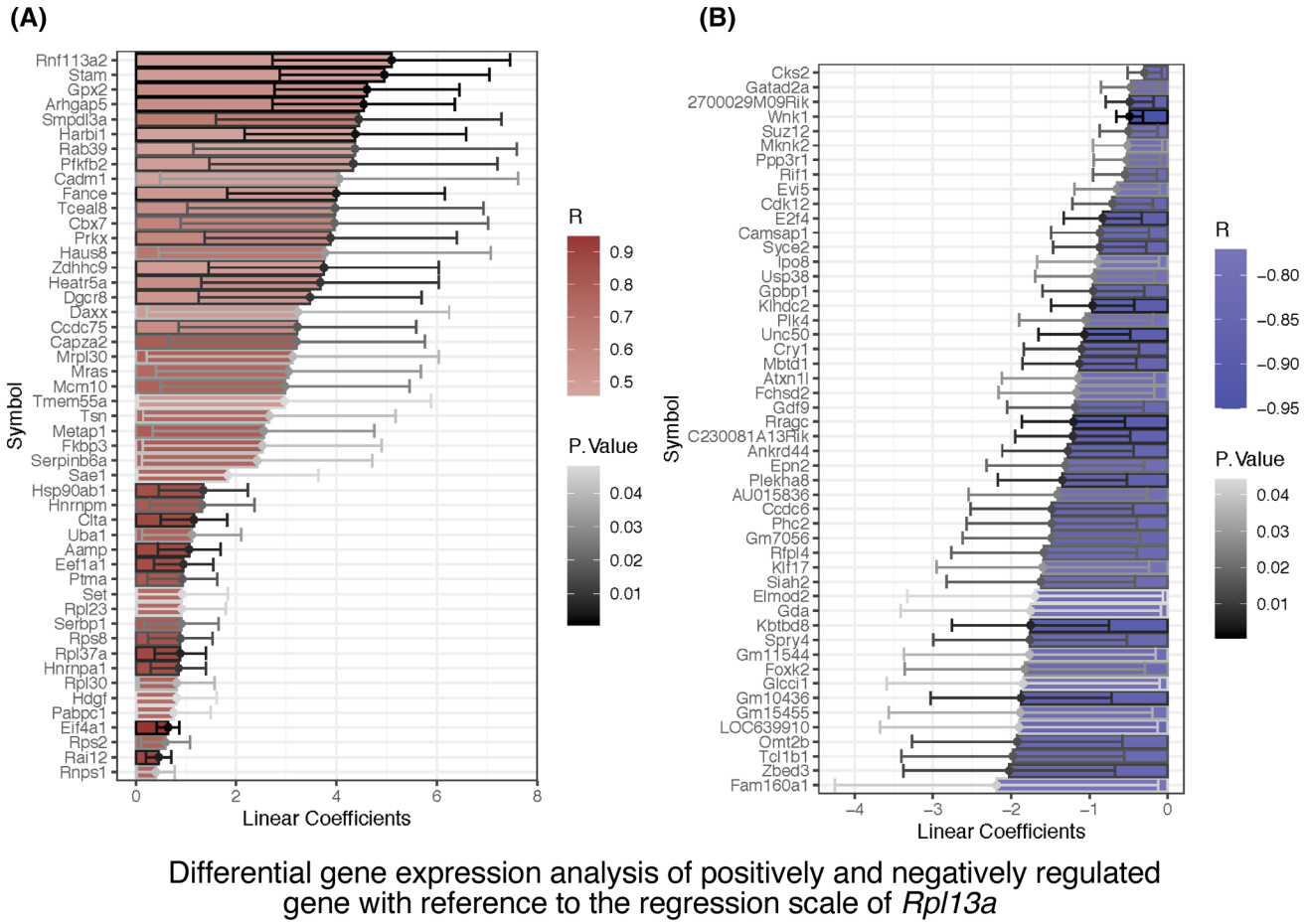

Differential gene expression analysis of positively and negatively regulated gene with reference to the regression scale of *Rpl13a*

FIGURE 2.

RNA sequencing analysis of *Rpl13a*−/− morulae reveals widespread alterations in gene expression. Plots, respectively, show the top 50 positively (A) and negatively (B) correlating genes with *Rpl13a* as measured by Pearson's *r*. Bars represent their linear regression coefficient estimates with 95% confidence intervals. The bar fill color represents their Pearson's "*r*" value, while bar outline color designates their normal coefficient "*p*" value.

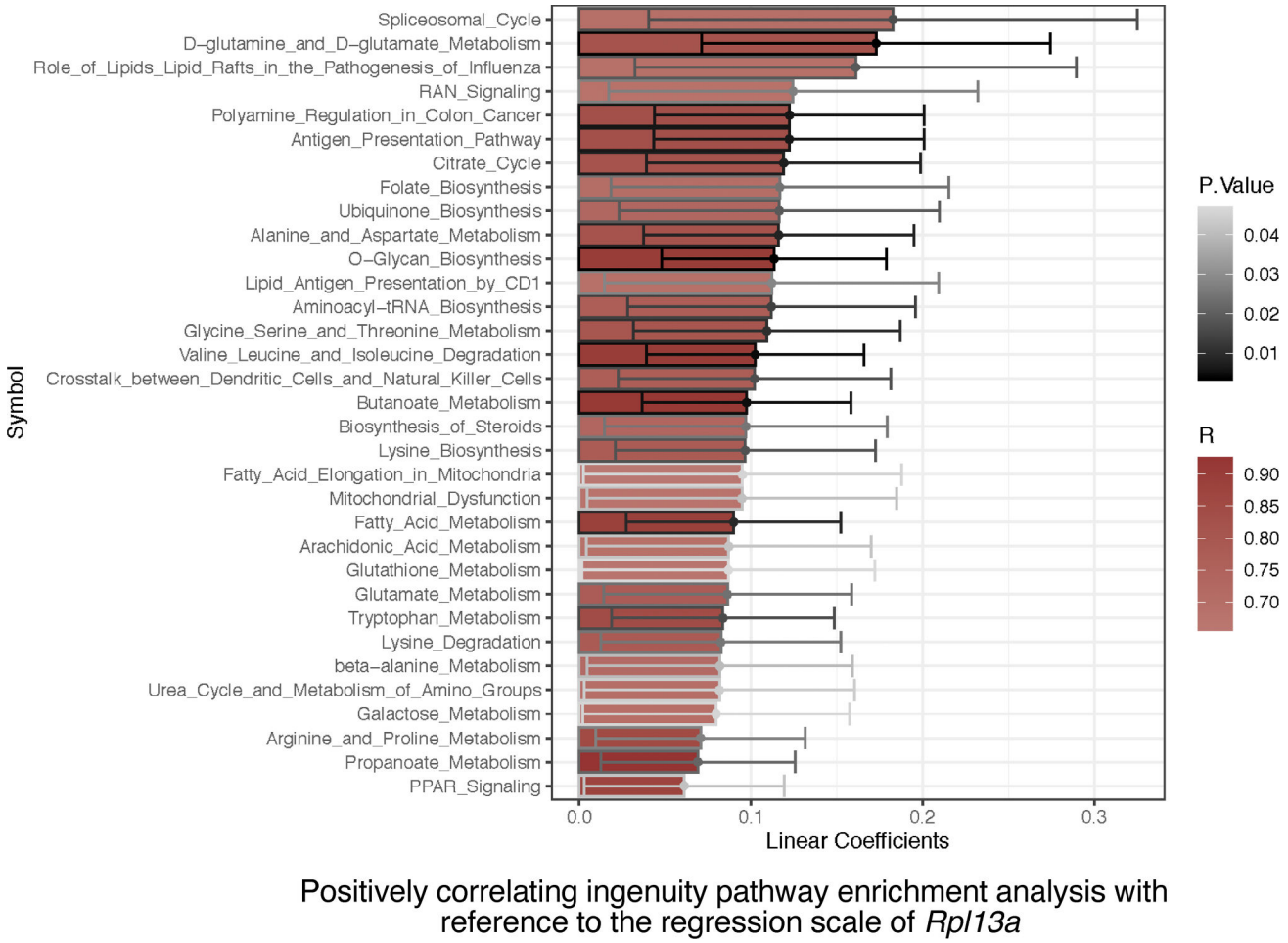

FIGURE 3.

Ingenuity pathway enrichment analysis of *Rpl13a*−/− morulae reveals important pathways. The plot shows positively correlating (by Pearson's *r*) ingenuity pathway enrichment passing a nominal $p < .05$ threshold when regressing against *Rpl13a*. Bars represent linear regression coefficient estimates with 95% confidence intervals. Bar fill color represents Pearson's "*r*" value, while bar outlines color designates the nominal coefficient "*p*" value.

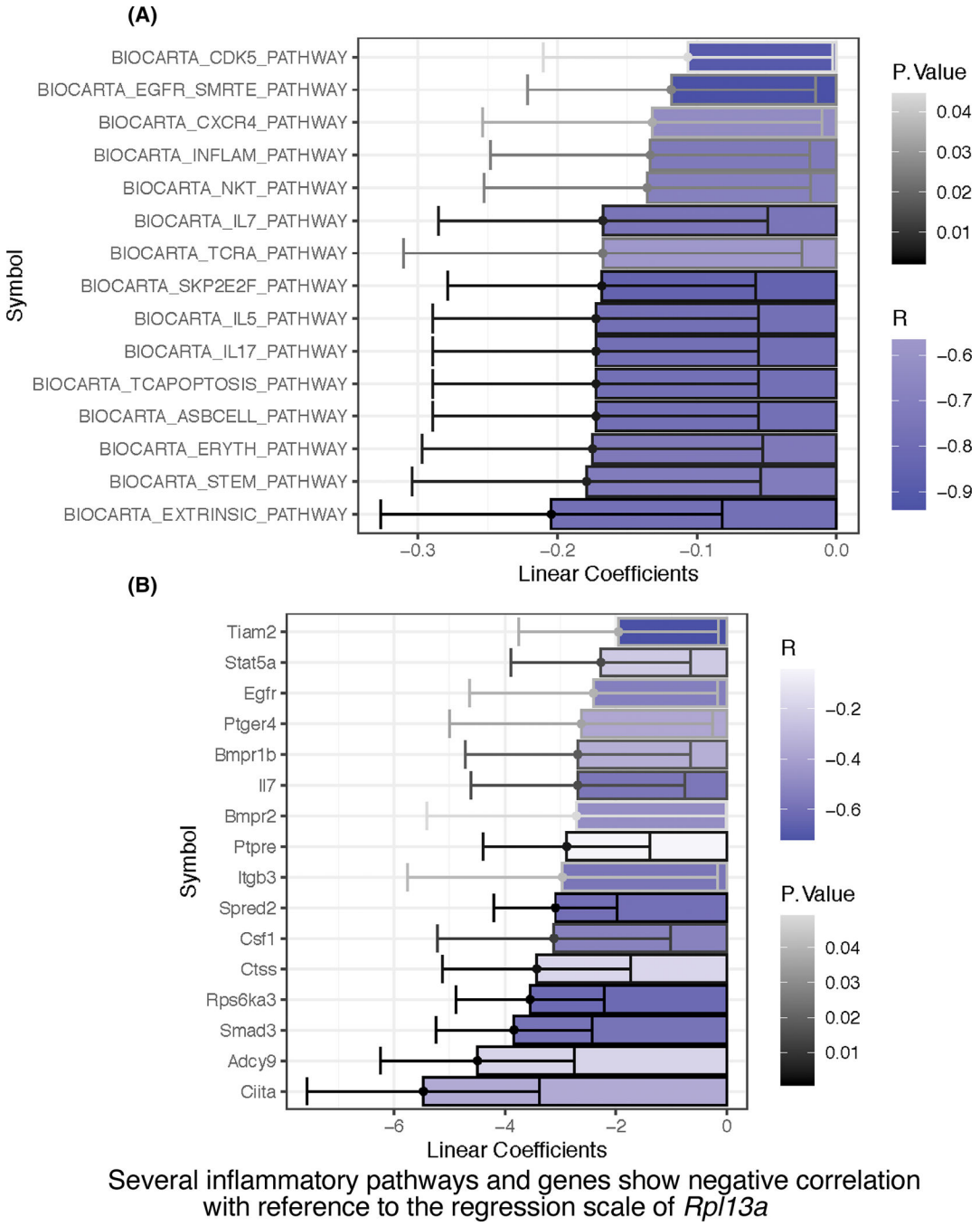

FIGURE 4.

Canonical pathway analysis of *Rpl13a*−/− morulae reveals an important role in inflammatory pathways. (A) The plot shows negatively correlating (by Pearson's *r*) MsigDB canonical pathways (BioCarta) passing a nominal $p < .05$ threshold when regressing against *Rpl13a*. Bars represent linear regression coefficient estimates with 95% confidence intervals. Bar fill color represents Pearson's *r* value, while bar outlines color designates the nominal coefficient *p*-value. (B) Plot shows select negatively correlating (by Pearson's *r*) macrophage inflammatory response genes passing a nominal $p < .05$ threshold when regressing against

Rpl13a. Bars represent linear regression coefficient estimates with 95% confidence intervals. Bar fill color represents Pearson's *r* value, while bar outline color designates nominal coefficient *p*-value.

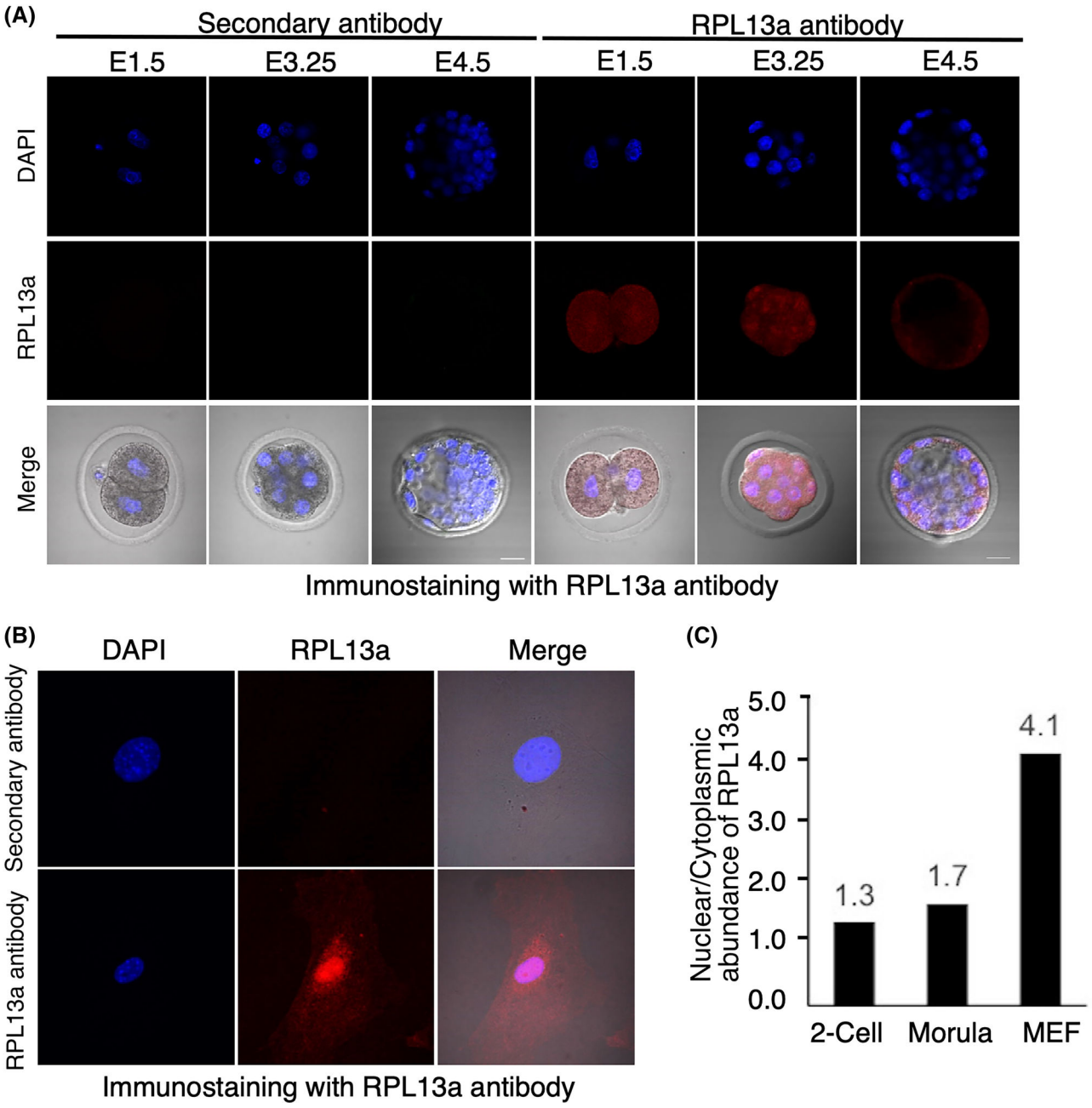

FIGURE 5.

RPL13a is localized to both the cytoplasm and nucleus in preimplantation embryos and mouse embryonic fibroblasts (MEF) cells. (A) Immunostaining of RPL13a at the two-cell (E1.5), early morula (E3.25), and blastocyst stages (E4.5); $n = 5$ embryos per stage. Embryos were counterstained with DAPI. As a negative control, embryos were treated with the secondary antibody alone; scale bar = 20 μm. (B) Immunostaining of RPL13a in MEF cells. As a negative control, cells were treated with the secondary antibody alone. (C) Relative intensity of nuclear RPL13a compared to cytoplasmic RPL13a in early embryos and MEFs. Signal intensity was measured with the image J program.

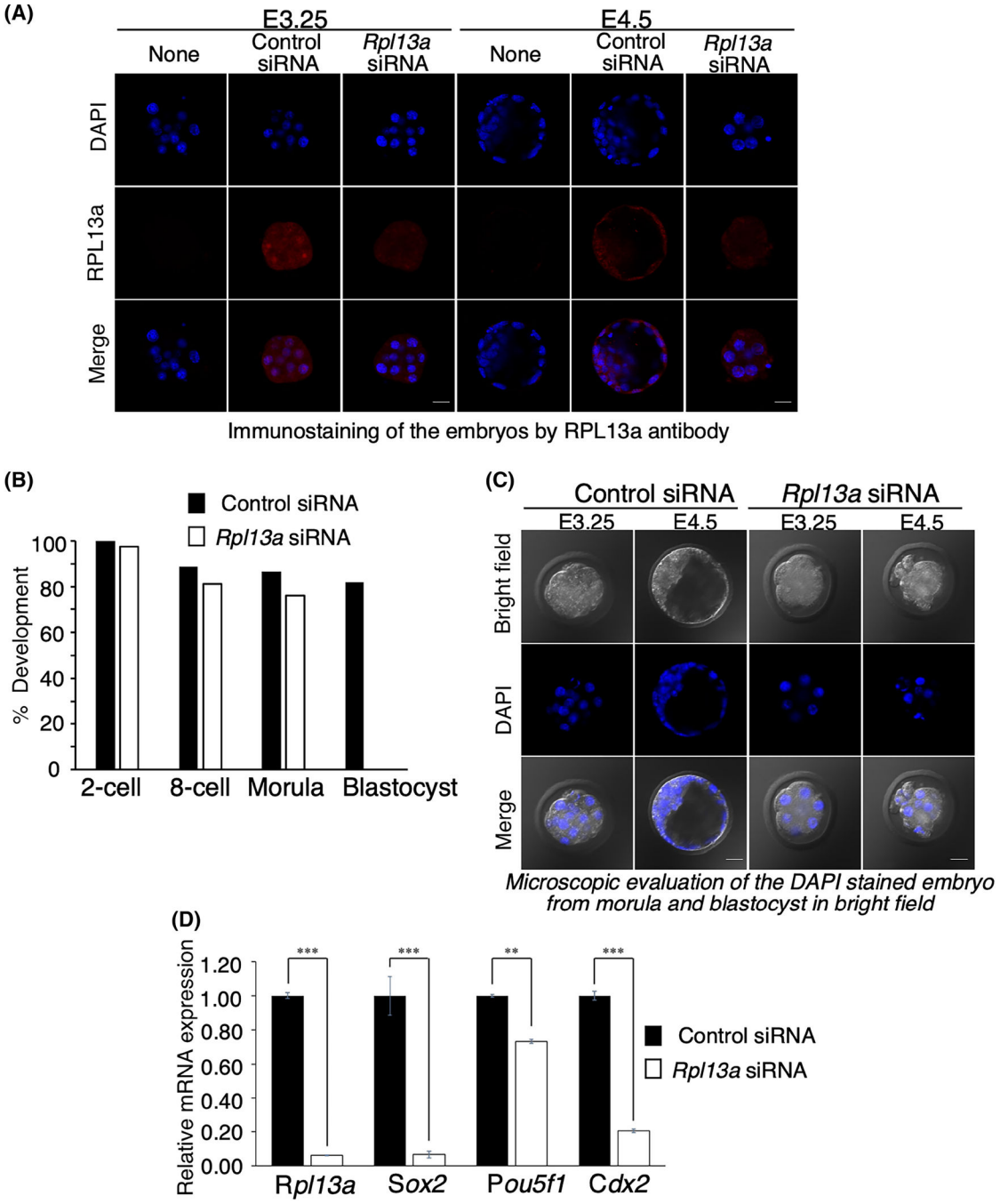

FIGURE 6.

RPL13a KD embryos arrest at the morula stage and exhibit altered lineage-specific gene expression. (A) Protein expression in RPL13a-depleted embryos was compared with embryos injected with control siRNA at E3.25 and E4.5; $n = 5$ embryos were evaluated per group. As a negative control, embryos were processed without primary antibodies. Embryos were counterstained with DAPI. An equivalent confocal optical section near the equator of a representative embryo was used to compare each group. Scale bar = 20 μm. (B) Percentage of control siRNA injected embryos ($n = 44$) and *Rpl13a* siRNA ($n = 42$) injected

embryos reaching the two-cell, eight-cell, morula, and blastocyst stages. Microinjection was conducted at the one-cell stage with 100 μM control and *Rpl13a* siRNA. (C) Morphological evaluation of morula and blastocyst stage embryos in control siRNA and RPL13a KD groups. Embryos were examined on embryonic day E3.25 and E4.5, Scale bar = 20 μm. Embryos were stained with DAPI. (D) Messenger RNA expression of lineage-specific transcription factors important for ICM and TE development was examined in control and RPL13a KD embryos at E3.25, *Ubtf* was used as a reference for the qRT-PCR control. Values are means ± SD. $^{**}p < .01$, $^{***}p < .001$. The experiment was repeated three times using $n = 20$ embryos per replicate; Student's *t*-test.

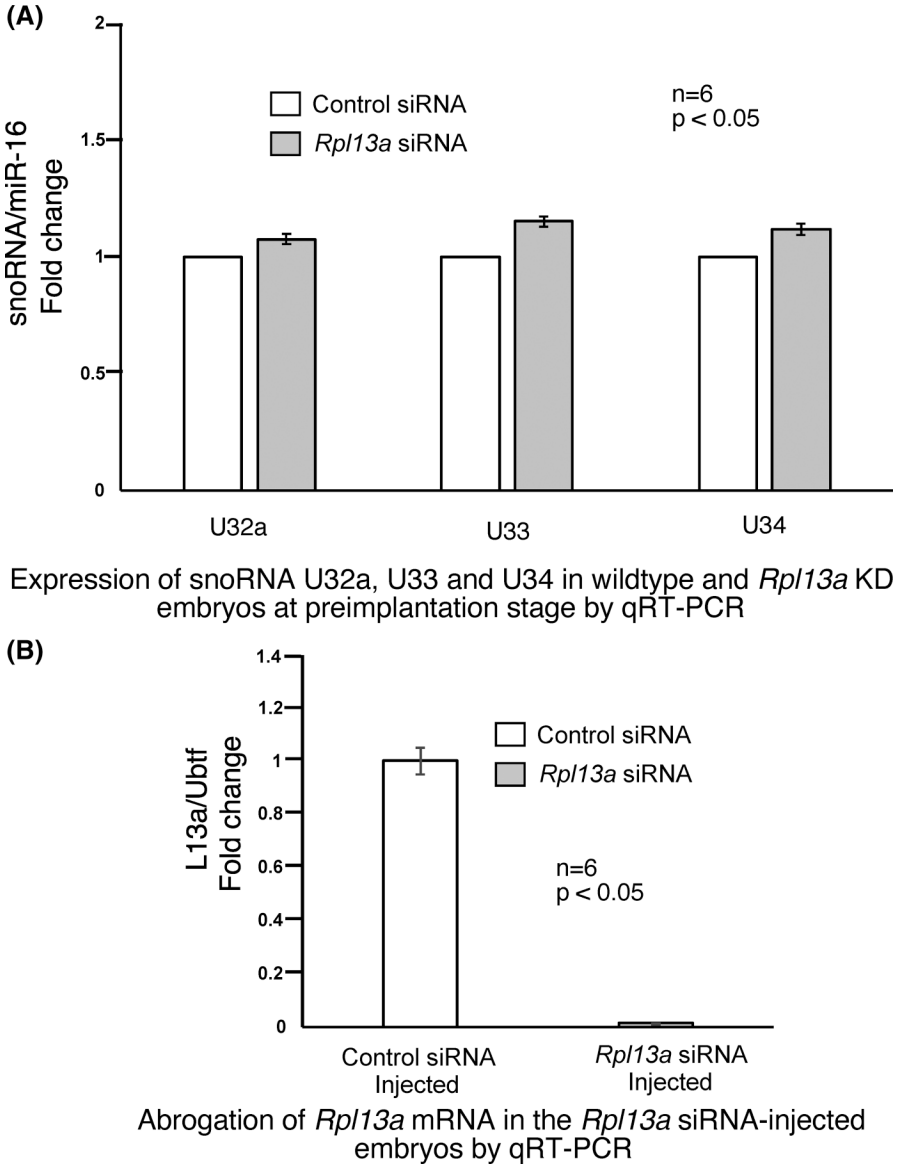

FIGURE 7.

RNAi-mediated depletion of *Rpl13a* does not abrogate the expression of snoRNAs U32a, U33, and U34. (A) Expression of snoRNAs U32a, U33, and U34 harbored in the *Rpl13a* intronic sequence were measured by qRT-PCR (SYBR Green), the upper panel. Expression was measured relative to miR-16 RNA as a reference. Quantification was performed in control siRNA injected-, and *Rpl13a* siRNA injected embryos at the morula stage. $n = 20$ embryos per replicate, $p < .05$. (B) From the same sample, the RNAi-mediated knockdown of *Rpl13a* transcripts was confirmed by qRT-PCR (SYBR Green) using *Ubtf* as a reference, $p < .05$). Data were derived from two biological replicates of control and siRNA-injected embryos. qRT-PCR was performed in triplicate; Student's *t*-test.

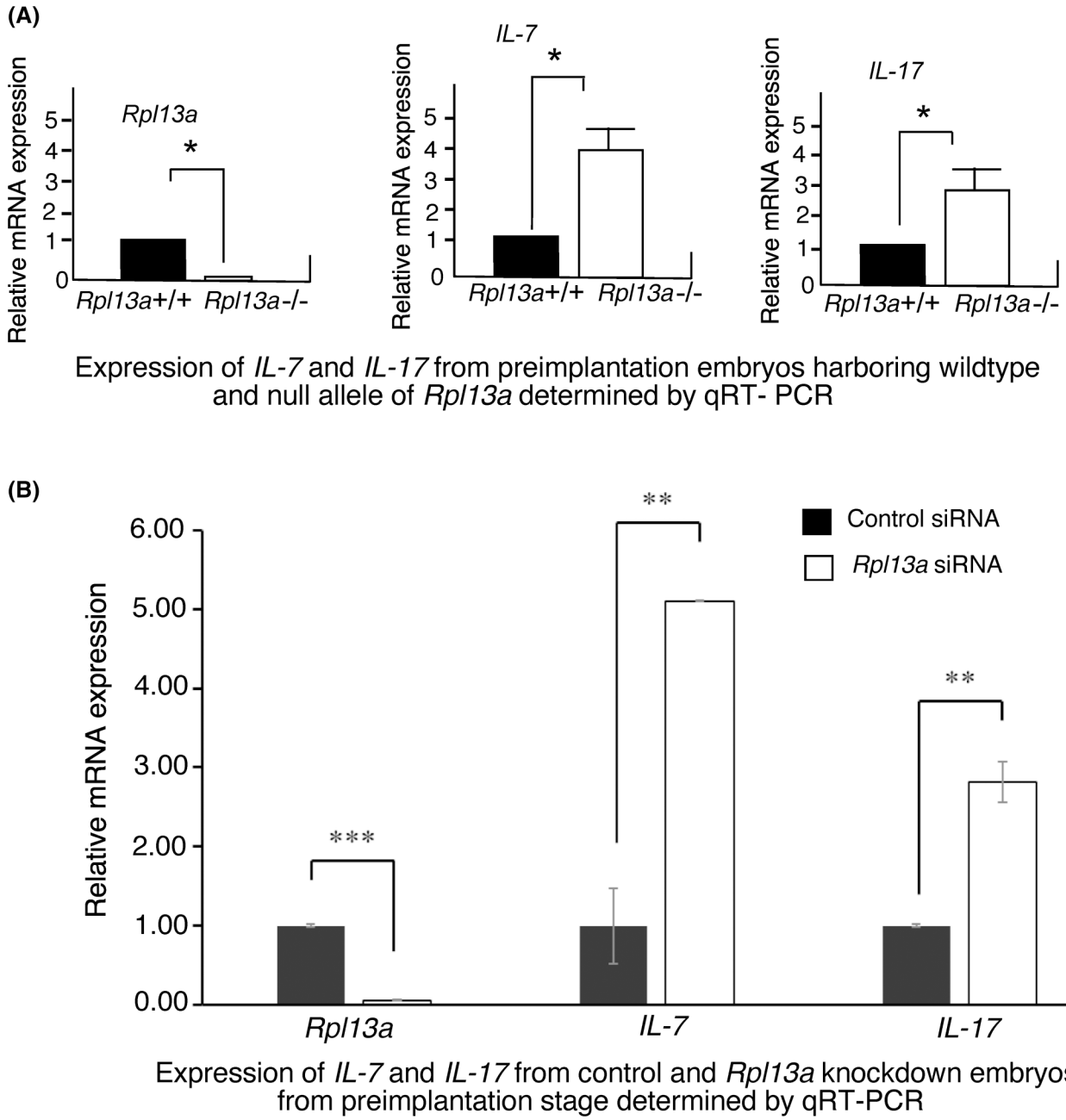

FIGURE 8.

A subset of inflammatory genes is upregulated in *Rpl13a*−/− and *Rpl13a* KD morula. (A) Elevated expression of *IL-7* and *IL-17* in homozygous *Rpl13a* KO morula (E3.0). Embryos were isolated on E3.0 from the cross between the mice with heterozygous null allele (*Rpl13a*+/−). Embryos harboring the wild type (*Rpl13a*+/+) and homozygous null allele (*Rpl13a*−/−) were identified by genotyping, and the RNA was subjected to qRT-PCR with specific primer for *IL-7* and *IL-17*. Abrogation of *Rpl13a* transcript level was also confirmed in the *Rpl13a*−/− embryos by qRT-PCR using *Rpl13a*-specific primer. Values are means ± SD. $p < .05$. The experiment was repeated three times using $n = 25$ embryos; Student's *t*-test. (B) Messenger RNA expression of *Rpl13a* and inflammatory genes was examined in

control and RPL13a KD embryos at E3.25. *Ubtf* was used as the housekeeping gene. Values are means ± SD. *$p < .05$, **$p < .01$, ***$p < .001$. The experiments were repeated three times using $n = 30$ embryos per replicate; Student's t-test.

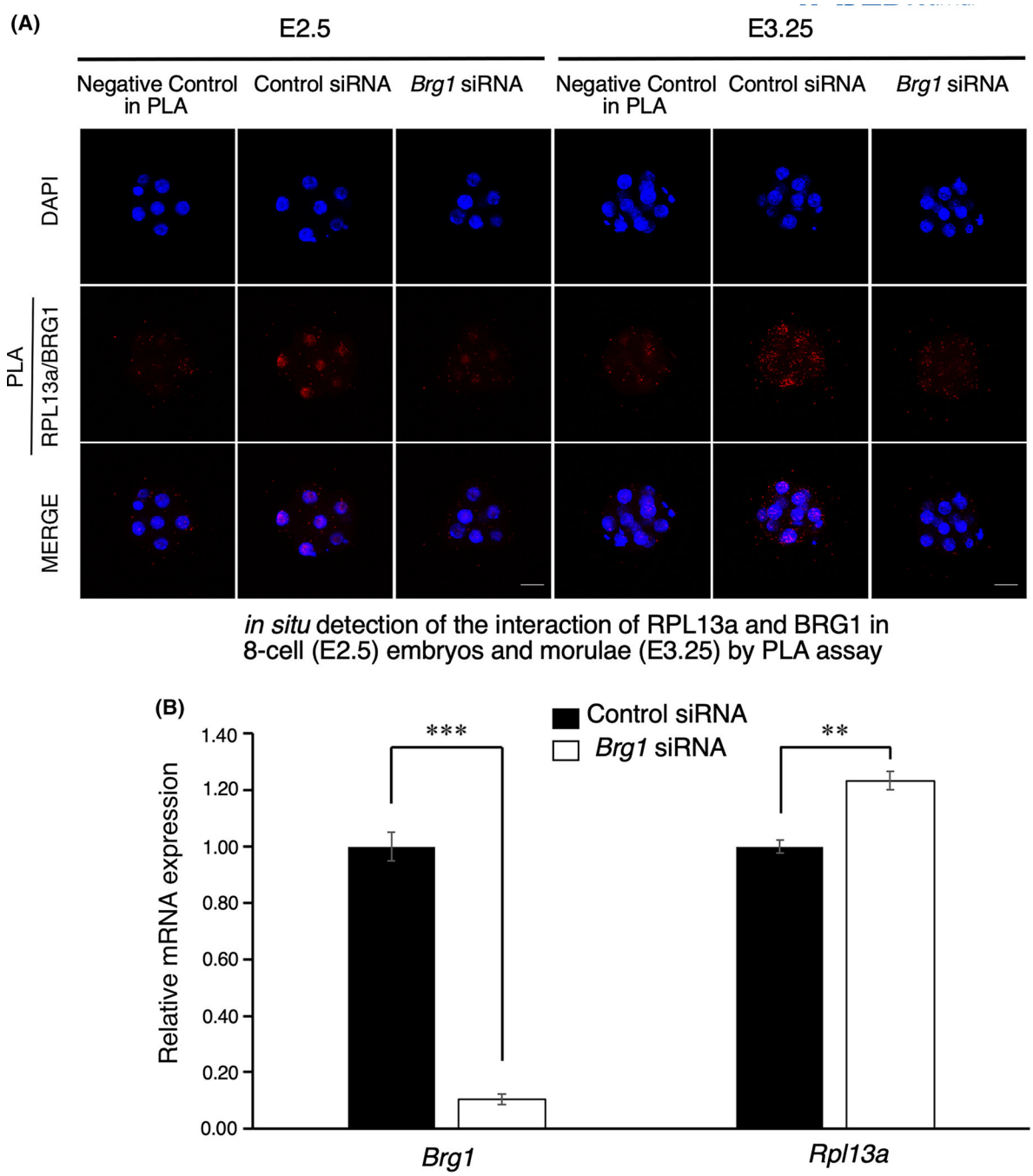

FIGURE 9.

RPL13a associates with chromatin during preimplantation embryo development. (A) PLA assay results of RPL13a and BRG1 interactions. PLA signal between RPL13a and BRG1 was evaluated in control siRNA ($n = 5$), and *Brg1* depleted embryos ($n = 5$) at the eight-cell (E2.5) and early morula (E3.25) stages. Five embryos from each group were tested. As a negative control, embryos were treated with the secondary antibody alone. For each experiment, equivalent confocal optical sections with *Z*-stack images of a representative embryo were used to compare each group. Scale bar = 20 μm. (B) Messenger RNA

expression of *Brg1* and *Rpl13a* in control and *Brg1* depleted embryos at the eight-cell (E2.5) and morula (E3.25). *Ubtf* was used as a housekeeping gene. Values are means ± SD. $^{**}p < .01$, $^{***}p < .001$. The experiment was repeated three times; Student's *t*-test.